Near-surface density currents observed in the stratocumulus-topped marine boundary layer

Matt Wilbanks[1], Sandra Yuter[1], Matthew Miller[1], Simon de Szoeke[2], Alan Brewer[3], Casey Burleyson[1,4]
[1]Department of Marine, Earth, and Atmospheric Sciences, North Carolina State University, Raleigh, NC, USA
[2]College of Oceanic and Atmospheric Sciences, Oregon State University, Corvallis, OR, USA
[3]National Oceanic and Atmospheric Association Earth Systems Research Laboratory, Boulder, CO, USA
[4]Pacific Northwest National Laboratory, Richland, WA, USA

ASR Atmospheric System Research

CP³g NC STATE UNIVERSITY Clouds and Precipitation Processes and Patterns Group

Introduction

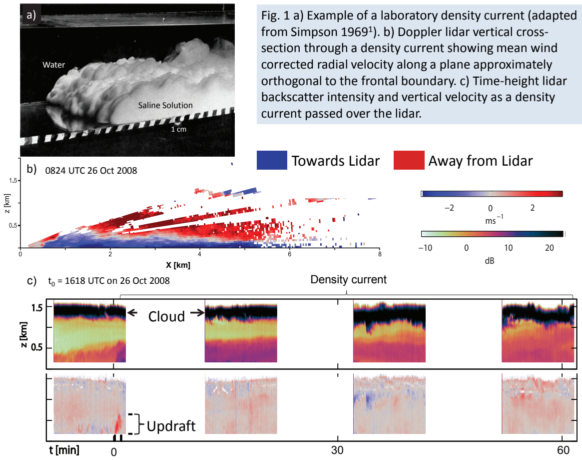

Fig. 1 a) Example of a laboratory density current (adapted from Simpson 1969[1]). b) Doppler lidar vertical cross-section through a density current showing mean wind corrected radial velocity along a plane approximately orthogonal to the frontal boundary. c) Time-height lidar backscatter intensity and vertical velocity as a density current passed over the lidar.

Drizzle-induced density currents (i.e. cold pools) are generated when evaporatively cooled, negatively buoyant air sinks to the earth's surface and diverges. They have been proposed to affect mesoscale circulation in marine stratocumulus.[2,3,4] Though studied extensively in mid-latitude continental deep convection[5,6,7,8], observational studies of density currents beneath marine stratocumulus are limited to aircraft data in a line or curtain.[9,10]

An objective method identified 71 density currents in 30 d of ship data collected during the 2008 VAMOS Ocean-Cloud-Atmosphere-Land Regional Experiment (VOCALS-REx) in the Southeast Pacific. Scanning Doppler lidar depictions of density currents and their prefrontal updrafts are presented for the first time beneath marine stratocumulus. The horizontal configuration of the surrounding clouds and drizzle, density current structure and kinematic features, as well as boundary layer conditions provide valuable context to address the potential role of density currents on mesoscale organization and drizzle cell convective initiation.

Density current distributions in met data

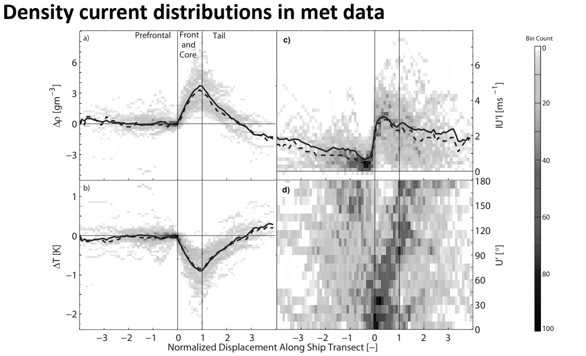

Fig. 2: Perturbation in ship a) air density, b) temperature, c) wind anomaly magnitude, and d) wind anomaly angular deviation (U'). U' is absolute value of the small angle between the wind anomaly and the 10-min average prefrontal wind. The solid (dashed) black line gives mean (median) values.

	ΔT [K]	h [m]	L [km]	t [min]	w [m s^{-1}]	C [m s^{-1}]
Range	0.2-2.1	80-610	5-40	8-161	0.28-1.51	0.2-5.1
Mean	0.8	330	15	33	0.9	1.8

Table 1: Density current temperature depression (ΔT), estimated depth (h) from lidar VADs, density current length along time-integrated ship transects (L), duration of density current in ship time series (t), mean vertical wind speed throughout prefrontal updraft (w), density current propagation speed (C) estimated by finding the magnitude of the resultant wind anomaly inside density current front zones.

Shelf clouds and prefrontal updrafts

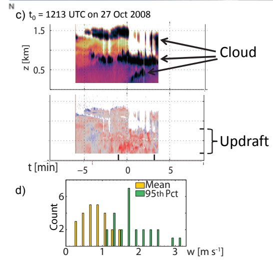

Fig. 3: a) Left: Panoramic photograph of a shelf cloud (within white brackets) seen along and directly above the density current front that approached from the east and crossed the ship at 1353 UTC. Right: Corresponding GOES VIS satellite, radar, and lidar PPI of mean wind corrected radial velocity. The white section line indicates the field of view of the photograph. b) Panorama of drizzle cell located above and adjacent to a density current as it approached the ship from the east (right plot as in a). c) Time-height lidar as the density current shown in b. passed over the lidar. e) Vertical velocity distributions from 25 lidar-observed prefrontal updrafts.

Diurnal Cycle and Mesoscale Cellular Organization

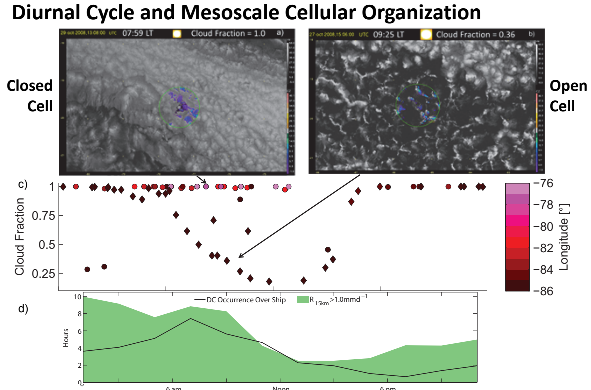

Fig. 4: Examples of closed cells (a) and open cells (b) in VIS satellite over the ship at the start of a density current. c) The relationship among local time of day, longitude, and the half-hourly cloud fraction over the ship at the start of each density current. Data points corresponding to density currents occurring on 26 Oct 2008 or 27 Oct 2008 –when a large region of predominantly open cells were observed—are diamond-shaped. The remaining data are indicated by circles. d) Diurnal cycle of enhanced local drizzle surrounding the ship (green) and times when a density current was detected over the ship (black line).

Effect of boundary layer shear

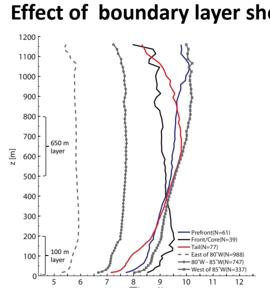

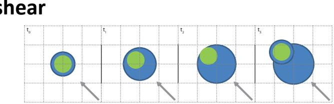

Fig. 5: Schematic of the development of a density current with an elongated tail oriented along the axis of the mean wind (gray arrow). The source drizzle cell (green) moves northwest at a marginally higher speed than the leading edge of the divergent cold pool (blue) and releases a second cold pool at t_3.

Fig. 6: Average lidar VAD wind speed profiles obtained within density current prefront, front/core, and tail zones compared with all VADs obtained within three different longitude categories.

Conclusions

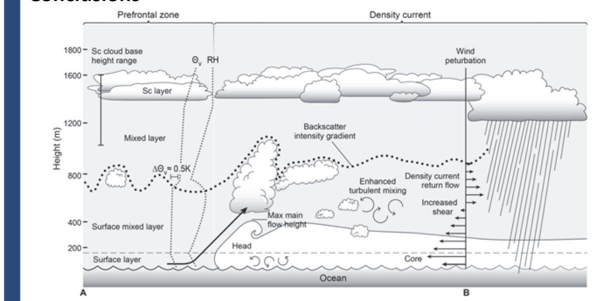

Fig. 7: Vertical cross-section along the axis of propagation of an idealized drizzle-induced near-surface density current.

- The observed density currents were on average 5-10 times thinner (330 m) and weaker (0.8 K) than typical continental thunderstorm cold pools.[5,8]
- Prefrontal updrafts were present immediately prior to and over top of nearly every density current, extending on average up to 800 m altitude.
- Shelf clouds capping the front edge of density currents frequently formed. These typically did not connect to the overlying stratocumulus deck.
- Density currents preferentially (34 out of 71) occurred within a region of predominantly open cells, but they also occurred beneath closed cells.
- Density current occurrence peaked in the morning between 06 and 08 LT, after the overnight peak in drizzle. The presence of enhanced local drizzle is not sufficient to explain the diurnal cycle of density current occurrence. Density currents were associated with subcloud dry layers and more dry static stability, which are more common during the day.
- Source drizzle cells and density current frontal boundaries approximately kept pace with each other because the differential speed of the cloud layer relative to the surface layer (1.9 m s^{-1}) was commensurate with density current propagation speed (1.8 m s^{-1}).
- Compared to front and core zones, density current tails had weaker density gradients, longer time-integrated ship transects, and stronger consistently positive vertical shear of wind speed in the lowest 800 m.

Diurnal cycle of subcloud stability

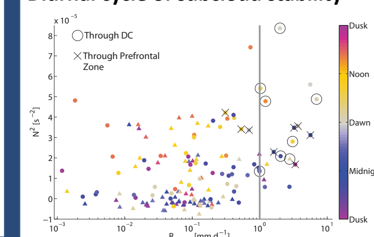

Fig. 8: Joint subcloud stability, time of day, and rain rate for periods with and without density currents. Subcloud stability is quantified using the sounding-derived squared dry Brunt-Väisälä frequency (N^2) calculated from the 100-m layer nearest the ocean surface to the 100-m layer just below the median cloud base. Data points collected east of 80°W are marked with triangles and points west of 80°W with circles.

References

1. Simpson, J. E., 1969: A comparison between laboratory and atmospheric density currents. Quart. J. Roy. Meteor. Soc.,95,758–765, doi:10.1002/qj.49709540609
2. Feingold, G., I. Koren, H. Wang, H. Xue, and W. A. Brewer, 2010: Precipitation-generated oscillations in open cellular cloud fields. *Nature*, **466,** 849–852, doi:10.1038/nature09314.
3. Savic-Jovcic, V., and B. Stevens, 2008: The structure and mesoscale organization of precipitating stratocumulus. *J. Atmos. Sci.*, **65,** 1587–1605, doi:10.1175/2007JAS2456.1.
4. 9. Wang, H., and G. Feingold, 2009: Modeling mesoscale cellular structures and drizzle in marine stratocumulus. Part II: The microphysics and dynamics of the boundary region between open and closed cells. *J. Atmos. Sci.*, **66,** 3257–3275, doi:10.1175/2009JAS3120.1.
5. Bryan, G. H., R. Rotunno, and J. M. Fritsch, 2007: Roll circulations in the convective region of a simulated squall line. J. Atmos. Sci., 64, 1249–1266, doi:10.1175/JAS3899.1.
6. Charba, J., 1974: Application of gravity current model to analysis of squall-line gust front. Mon. Wea. Rev., 102, 140–156, doi:10.1175/1520-0493(1974)102<0140:AOGCMT>2.0.CO;2.
7. Goff, C.R., 1976: Vertical structure of thunderstorm outflows. Mon. Wea. Rev., 104, 1429–1440, doi:10.1175/1520-0493(1976)104<1429:VSOTO>2.0.CO;2.
8. Engerer, N. A., D. J. Stensrud, and M. C. Coniglio, 2008: Surface characteristics of observed cold pools. Mon. Wea. Rev., 136, 4839–4849, doi:10.1175/2008MWR2528.1.
9. Jensen, J. B., S. Lee, P. B. Krummel, J. Katzfey, and D. Gogoasa, 2000: Precipitation in marine cumulus and stratocumulus: Part I: Thermodynamic and dynamic observations of closed cell circulations and cumulus bands. Atmos. Res., 54, 117–155, doi:10.1016/S0169-8095(00)00040-5.
10. Terai, C. R., and R. Wood, 2013: Aircraft observations of cold pools under marine stratocumulus. Atmos. Chem. Phys., 13, 9899-9914, 2013, doi: 10.5194/acp-13-9899-2013.

Acknowledgements: This research was supported by the Office of Science (Biological and Environmental Research) U.S. Department of Energy Grants DE-SC0006701 and DE-SC0006994, the National Oceanic and Atmospheric Administration (NOAA) Climate Program Office (CPO) Climate Prediction Program for the Americas (CPPA) Grants GC09-252b and GC09-507, and the National Aeronautics and Space Administration Grant NNX11AE98G.